



This is a repository copy of *Geodesically smoothed tensor features for pulmonary hypertension prognosis using the heart and surrounding tissues*.

White Rose Research Online URL for this paper:
<http://eprints.whiterose.ac.uk/163177/>

Version: Accepted Version

Proceedings Paper:

Uthoff, J., Alabed, S., Swift, A.J. et al. (1 more author) (2020) Geodesically smoothed tensor features for pulmonary hypertension prognosis using the heart and surrounding tissues. In: Martel, A.L., Abolmaesumi, P., Stoyanov, D., Mateus, D., Zuluaga, M.A., Zhou, S.K., Racoceanu, D. and Joskowicz, L., (eds.) Medical Image Computing and Computer Assisted Intervention – MICCAI 2020. 23rd International Conference on Medical Image Computing & Computer Assisted Intervention (MICCAI 2020), 04-08 Oct 2020, Lima, Peru. Springer Nature Switzerland , pp. 253-262. ISBN 9783030597122

https://doi.org/10.1007/978-3-030-59713-9_25

This is a post-peer-review, pre-copyedit version of an article published in Martel A.L. et al. (eds) Medical Image Computing and Computer Assisted Intervention – MICCAI 2020. MICCAI 2020. Lecture Notes in Computer Science, vol 12262. The final authenticated version is available online at: http://dx.doi.org/10.1007/978-3-030-59713-9_25

Reuse

Items deposited in White Rose Research Online are protected by copyright, with all rights reserved unless indicated otherwise. They may be downloaded and/or printed for private study, or other acts as permitted by national copyright laws. The publisher or other rights holders may allow further reproduction and re-use of the full text version. This is indicated by the licence information on the White Rose Research Online record for the item.

Takedown

If you consider content in White Rose Research Online to be in breach of UK law, please notify us by emailing eprints@whiterose.ac.uk including the URL of the record and the reason for the withdrawal request.



eprints@whiterose.ac.uk
<https://eprints.whiterose.ac.uk/>

Geodesically Smoothed Tensor Features for Pulmonary Hypertension Prognosis using the Heart and Surrounding Tissues

Johanna Uthoff¹, Samer Alabed², Andrew J. Swift^{2,3}, and Haiping Lu^{1,3}

¹ Department of Computer Science, The University of Sheffield, UK

² Sheffield Teaching Hospitals NHS Foundation Trust, Sheffield, UK

³ INSIGNEO, Institute for In Silico Medicine, The University of Sheffield, UK
j.uthoff@sheffield.ac.uk

Abstract. Cardiac magnetic resonance imaging (CMRI) provides non-invasive characterization of the heart and surrounding tissues. It is an important tool for the prognosis of pulmonary arterial hypertension (PAH), a disease with heterogeneous presentation that makes survival likelihood prediction a challenging task. In this paper, we propose a **Geodesically Smoothed Tensor** feature learning method (GST) that utilizes not only the heart but also its surrounding tissues to characterize disease severity for improving prognosis. Specifically, GST includes structures surrounding the heart by geodesic rings which were incrementally smoothed with Gaussian filters. This provides additive insight while modulating for patient positional differences for a subsequent tensor-based feature learning pipeline. We performed evaluation on Four Chamber and Short Axis CMRI from 150 individuals with confirmed PAH and 1-year mortality census (27 deceased, 123 alive). The proposed GST method improved AUC and Cox difference at 4-years post-imaging (Cox4YD) over the standardized measurement of right ventricular end systolic volume index (RVESVi: AUC: 0.58; Cox4YD: 0.18) on the Four Chamber protocol (AUC: 0.77; Cox4YD: 0.35). Only AUC was improved over RVESVi in the Short Axis scans (AUC: 0.77; Cox4YD: 0.16).

1 Introduction

Pulmonary arterial hypertension (PAH) is a severe disease affecting the cardiopulmonary system with a recorded 1-year mortality rate of 15% [3]. The heterogeneous nature of disease presentation and the diversity in disease progression at time-of-diagnosis makes predicting survival likelihood and proper treatment planning a challenging task for PAH [9]. Guidelines from the European Society of Cardiology and the European Respiratory Society assigns categorical risk of 1-year mortality to subjects based on assessment of symptom severity, 6-minute walk test, and right ventricle function [6]. There is evidence that prognostic indicators including clinical, echo-cardiogram imaging, and right heart catheterization (RHC) can be used to predict a subject’s likelihood of mortality [2]. Recently, standardized cardiac magnetic resonance imaging (CMRI) measures

calculated from user-delineated contours were shown to have prognostic value in PAH subjects when combined with clinical measures (AUC = 0.70-0.78) [8].

Prior studies of artificial intelligence technologies for PAH prognosis have focused on segmentation-based ventricular volume and motion analysis and achieved a moderate performance accuracy (AUC = 0.75) [1]. From related literature, while feature extraction methods typically focus on specific regions of interest within a dataset, there are potentially features in non-target organ regions which could provide additional disease risk classification [15]. Inspired by this, we note that features from the surrounding tissues of the heart has the potential to benefit PAH prognosis. For example, PAH subjects with worse outcomes tend to have increased pulmonary vasculopathy [7] which could potentially be detected as features in the lungs. However, the automatic extraction of meaningful features from areas external to the heart is challenged by the diversity in patient positioning during scanning. As the priority of the imaging technician is the location of heart structures, the positioning of secondary structures (lungs, liver, appendages) may be inconsistent or difficult to align to a standard.

Moreover, temporal-spatial medical scans, such as CMRIs have high dimensionality characterizing the in-vivo tissue conditions of target organs and surrounding structures. However, the number of available samples is much smaller relevant to such high dimensionality, making machine learning challenging on such data. Recently, a tensor-based dimensionality reduction method named as multilinear principal component analysis (MPCA) [10] has shown promising results in automated diagnosis of PAH by detecting interpretable tensorial CMRI features [13]. It will be interesting to explore its application in prognosis.

Contributions: This paper proposes a **Geodesically Smoothed Tensor** feature learning method (GST) for PAH prognosis. More specifically, we use a simple, regional Gaussian smoothing to include tissues surrounding the heart incrementally. This has the potential to alleviate the challenges associated with positional discrepancies and promote a more comprehensive assessment of mortality risk. The geodesically smoothed CMRI is then passed to a tensor feature learning pipeline to predict the mortality. To the best of our knowledge, this is the first work to employ incremental geodesic-based image smoothing and investigate the prognostic value of tensor-based features from such smoothed images.

2 Methodology

Figure 1 shows an overview of the proposed GST pipeline for PAH prognosis. Source code is made available at <https://github.com/pykale>.

CMRI Data Preprocessing. Image preprocessing is consisted of (1) CMRI unit standardization, (2) magnetic field in-homogeneity bias correction, (3) inter-subject scan alignment, (4) incremental geodesic distance smoothing, and (5) in-plan resolution down-sampling. CMRI units were standardized using z-score normalization to allow for meaningful comparison between subjects [11]. CMRI

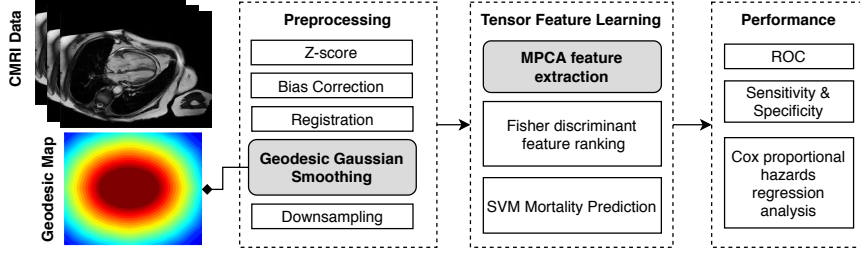


Fig. 1: Overview of the proposed pipeline for PAH prognosis including geodesic smoothing preprocessing, tensor feature learning, and performance analysis. Gray highlighted regions are described in more detail in the Methods.

field in-homogeneity bias correction was performed using the N4ITK method to correct for acquisition artifacts [14]. Affine registration of three landmarks points placed by an expert in each of the datasets was performed to align subject hearts to the same image space; specific landmarks are detailed in the CMRI Scan Data section of the Experiments. Incremental geodesic distance smoothing is described in the next section. The in-plane scaling was done by max-pool at 2, 4, 8, 16 times resulting in down-sampled resolution images of 256×256 , 128×128 , 64×64 , and 32×32 respectively.

Geodesic Smoothing. Our GST method performs incremental smoothing based on geodesic distance from the region of the heart using iterative mask dilation and Gaussian filters. Let H_i be the previous iteration i 's mask with diameter d_{H_i} , ρ be the width of the concentric shell, s be the structuring element $4\pi\rho^2$, and X_m be indicating a phase in subject's cardiac cycle.

First we calculate the geodesic distance using dilation procedure from the edge of the initial mask H_i to the concentric edge at an expanding distance ρ towards the image bounds, hereby H_{i+1} follows the formulation:

$$H_{i+1} = H_i \oplus s. \quad (1)$$

The initial mask, H_i is subtracted from the dilated mask and element-wise multiplication is performed with image X_m . This results in a shell of image about the H_i , V_i , with inner diameter of d_{H_i} and outer diameter of $d_{H_i} + 2 \times \rho$, calculated as:

$$V_i = (H_{i+1} - H_i) \odot X_m. \quad (2)$$

The 2D Gaussian of V_i is calculated as W_i . Let σ be the smoothing factor. The formulation of W_i is as follows:

$$W_i = G[V_i(r, c)|\sigma] = \frac{1}{2\pi\sigma^2} e^{-\frac{r^2+c^2}{2\sigma^2}}, \quad (3)$$

which is updated for each i with $\Delta\sigma$ as the defined incremental increase in smoothing factor as:

$$\sigma = \sigma + \Delta\sigma. \quad (4)$$

Equations (1) to (4) are repeated until H_{i+1} has reached the image boundaries ($i = I$). Finally, the incrementally smoothed image X'_m is calculated as the sum of all W_i as follows:

$$X'_m = \sum_{i=0}^I W_i. \quad (5)$$

The resulting X'_m is an image of the same size as X_i . The original masked heart region is unchanged from the original image and voxels along tangential arrays from the mask become increasingly more blurred. The lower left of Fig. 1 shows a typical mask and Fig. 2B shows an example on a Four Chamber scan.

Tensor Feature Learning. The learning of prognostic tensor features involves (1) MPCA feature extraction, (2) Fisher discriminant feature ranking, (3) support vector machine (SVM) training, and (4) cross validation. After CMRI data preprocessing, MPCA is applied to the aligned dataset for spatial-temporal feature extraction - see next section for details on the parameters for *Baseline*, *Masked*, *Surrounding Smoothing*, and *Geodesic Smoothing*. After MPCA, the extracted features are ranked using Fisher’s discriminant score. Those top-ranked features were utilized to train a linear SVM through 10-fold *stratified* cross validation with class imbalance preserving fold generation. This was repeated 10 times for a 10×10-fold cross validation to help alleviate bias from random fold generation and increase the estimation reliability for small sample size.

Spatial-Temporal Feature Extraction. We identify prognostic characteristics by using MPCA [10] to learn multilinear bases from image stacks to obtain low-dimensional tensor features. Here, we represent our M CMRI samples as third-order tensors in the form $\{X_1, \dots, X_M \in \mathbb{R}^{I_1 \times I_2 \times I_3}\}$. MPCA utilizes these inputs to extract low-dimensional tensor features $\{Y_1, \dots, Y_M \in \mathbb{R}^{P_1 \times P_2 \times P_3}\}$ by learning three (order $N = 3$) projection matrices $\{\mathbf{U}^{(n)} \in \mathbb{R}^{I_n \times P_n}, n = 1, 2, 3\}$ as follows:

$$Y_m = X_m \times_1 \mathbf{U}^{(1)\top} \times_2 \mathbf{U}^{(2)\top} \times_3 \mathbf{U}^{(3)\top}, m = 1, \dots, M, \quad (6)$$

where $P_n < I_n$, thereby reducing the dimension of the input tensor to $P_1 \times P_2 \times P_3$ from $I_1 \times I_2 \times I_3$. The projection matrices $\{\mathbf{U}^{(n)}\}$ are optimized through maximizing the total scatter $\Psi_Y = \sum_{m=1}^M \|Y_m - \bar{Y}\|_F^2$, where $\bar{Y} = \frac{1}{M} \sum_{m=1}^M Y_m$ is the mean tensor and $\|\cdot\|_F$ is the Frobenius norm [10]. MPCA has one hyperparameter Q determining the tensor subspace dimensions $\{P_1, P_2, P_3\}$ and its default setting takes only one iteration.

Performance Assessment. Model performance was evaluated using 10×10-fold cross validation. The primary metric is the area under the receiver-operator

Table 1: Demographic and clinical information of study population. *N*: number of subjects; *IPAH*: idiopathic PAH; *WHO*: World Health Organization.

Attribute	Deceased	Alive	<i>p</i>
<i>N</i>	27	123	-
IPAH	14 (52%)	55 (44%)	0.62
Female	17 (63%)	88 (72%)	0.56
Age (Mean±STD)	70.3 ± 10.4	62.2 ± 12.7	< 0.01
WHO-2	0 (0%)	7 (6%)	
WHO-3	23 (85%)	103 (84%)	0.49
WHO-4	4 (15%)	13 (10%)	

characteristic curve (AUC). We computed both sensitivity and specificity. We also performed Cox proportional-hazards regression [4,12], a type of non-parametric survival analysis which relates variables to survival time; the measured effect is the *Hazard rate* which is the expected number of events/deaths per unit time. Categorical variables were assessed with Fisher’s Exact Test or Chi-squared test and continuous variables were assessed with Wilcoxon Rank Sum test, (R, <https://www.r-project.org/>).

3 Experiments

For the task of PAH prognosis assessment, the proposed pipeline takes as input CMRI data represented by volumetric slices (spatial) of intensity units over 20 phases of the cardiac cycle (temporal).

Study Population. Subjects diagnosed with PAH and imaged prior to treatment with CMRI between December 2014 and February 2017 were included in this study following institutional review board approval and ethics committee review. In total, 150 subjects were included in this study; diagnosis of PAH was made following RHC within 48 hours of imaging. Table 1 lists key demographics and clinical information for the study subjects. Subjects were censused in November 2019 at which time 80 subjects (52%) were alive. One-year mortality was calculated from date of imaging, with a total 27 subjects (18%) deceased within one year of CMRI assessment. The median survival time of those who died within 1-year was 173 days. Subjects who were deceased after 1-year tended to be older (70 years average) compared to those who were alive at 1-year follow-up (62 years average).

CMRI Scan Data. Two CMRI protocols - Short Axis and Four Chamber - were utilized in this study. All scans were performed on a 1.5 Tesla GE HDx (GE Healthcare, Milwaukee, USA) using an 8-channel cardiac coil and retrospective electrocardiogram gating. Acquisition parameters followed clinical standards with a cardiac gated multi-slice balanced SSFP sequence (20 frames per cardiac cycle, slice thickness 8mm, FOV 48, matrix 512 x 512, BW 125 KHz/pixel,

TR/TE 3.7/1.6 ms). Expert reader defined landmarks were selected as the inferior hinge point, superior hinge point, and interolateral inflection point of right ventricular free wall for the Short Axis scan. For the Four Chamber the left ventricular apex, mitral annuli, and tricuspid annuli were used.

CMRI Tensor Experimental Setup. Four experimental levels were explored on both the Four Chamber and Short Axis datasets: (1) *Baseline*, (2) *Masked*, (3) *Gaussian Surroundings*, and (4) *Gaussian Geodesic*.

- The *Baseline Tensor* experiment took as input the complete unmasked CMRI and tensor feature extraction was performed on all voxels.
- The *Masked Tensor* experiment took as input CMRI with a user-defined ellipse circumscribing the heart and tensor feature extraction was performed on voxels within the masked heart region.
- The *Surrounding Smoothing Tensor (SST)* experiment took as input CMRI Gaussian smoothing performed on all voxels exterior to the ellipsoid mask with two levels of $\sigma = [0.5, 1.0]$ and tensor feature extraction was performed on all voxels.
- The *Geodesic Smoothing Tensor (GST)* experiment took as input CMRI with Gaussian smoothing performed with incremental increases on all voxels exterior to the ellipsoid mask with two levels of $\sigma = [0.5, 1.0]$, one level of incremental $\sigma_i = 0.1$, and two levels of concentric size $bw = [5, 10]$ and tensor feature extraction was performed on all voxels.

For all the experiments, in-plane scaling was done by max-pool at 2, 4, 8, 16 times resulting in down-sampled resolution images of 256×256 , 128×128 , 128×128 , and 32×32 respectively.

Comparison Studies. Contour-based measurements of the right ventricle end-diastolic volume index (RVEDVi) and right ventricle end-systolic volume index (RVESVi) were made by an expert reader and thresholded based on published categories [8].

Classification Accuracy. Table 2 shows the performance results from experiments. The RVEDVi and RVESVi measures both achieved relatively low performance (AUC = 0.577-0.581). Performance improvement was seen with application of all tensor-based experiments over *Baseline Tensor*. In Four Chamber *Masked Tensor*, binary masking improved prediction quality by a difference of 0.12 in AUC. Minimal difference ($\Delta AUC < 0.01$) was seen by applying a constant Gaussian smoothing over the surrounding structures (*SST*). However, use of *GST* to incrementally increase the level of σ farther away from the heart improved performance by up to 0.07 difference in AUC. The best performing (AUC = 0.774) prognostic tool was the Four Chamber *GST* which extracted tensor features from the heart and concentric rings of 5-voxel steps increasing the level of blur sigma from 0.5 by 0.1 each step. On the Short Axis *Masked Tensor*, an improvement of 0.20 points in ΔAUC was achieved. Only modest improvement ($\Delta AUC = 0.01$) was seen in the Short Axis *GST*.

Table 2: Experimental classification settings and results. The best results were in bold for the last three columns. Precision is shown as two decimal places therefore some tied values in the table differ in the third digit (e.g. 0.58 and 0.77). *AUC*: area-under-curve for 1-year mortality; *SENS*: sensitivity for 1-year mortality; *Cox4YD*: Cox Proportional-Hazards Regression difference at 4-years after imaging; *RVEDVi*: right ventricular end-diastolic volume index; *RVESVi*: right ventricular end-systolic volume index; *SST*: Surrounding Smoothed Tensor; *GST*: Geodesic Smoothed Tensor.

	Experiment	Mask	Gaussian	Geodesic	AUC	SENS	Cox4YD
Standard	RVEDVi	-	-	-	0.58	0.52	0.02
	RVESVi	-	-	-	0.58	0.74	0.18
Four Chamber	Baseline	-	-	-	0.60 ± 0.03	0.52	0.16
	Masked	YES	-	-	0.70 ± 0.03	0.59	0.18
	SST	YES	0.5	-	0.71 ± 0.02	0.67	0.19
	SST	YES	1.0	-	0.70 ± 0.03	0.67	0.22
	GST	YES	0.5	5	0.77 ± 0.03	0.70	0.35
	GST	YES	1.0	10	0.77 ± 0.03	0.70	0.34
Short Axis	Baseline	-	-	-	0.56 ± 0.04	0.44	0.02
	Masked	YES	-	-	0.75 ± 0.03	0.70	0.15
	SST	YES	0.5	-	0.71 ± 0.02	0.70	0.11
	SST	YES	1.0	-	0.63 ± 0.03	0.59	0.08
	GST	YES	0.5	5	0.76 ± 0.03	0.78	0.16
	GST	YES	1.0	10	0.73 ± 0.03	0.70	0.15

Cox Proportional-Hazards Regression Analysis. Cox regression analysis was performed on the top prognostic predictions - with Kaplan-Meier survival curves shown in Figure 2A [5]. The Four Chamber *GST* had the hazards ratio (HR) of 2.89 (CI: [1.81, 4.63], $p < 0.01$), with good discrimination between survival curves beyond 365 days. Similar results were seen for the Short Axis *GST* (HR 1.81, [1.13, 2.90], $p = 0.01$). The CMRI standardized score of *RVESVi* categorized into low and intermediate-high score achieved a non-significant hazards (HR 1.70, [1.01, 2.88], $p = 0.05$). The WHO functional class clinical score also achieved high odds (HR 2.00, [1.17, 3.43], $p = 0.01$), however this is likely unrealistically biased by the absence of deceased subjects at time of census who were WHO category-2. A comparison of the difference at 4-years survival rates for predicted-deceased and predicted-survived, shown graphically in Fig. 2A, is included in Table 2 as column Cox4YD.

Uni-variate Cox indicated statistical significance ($p < 0.05$) in (1) Age, (2) WHO functional class, (3) Four Chamber *GST* 1-year mortality prediction, and (4) Short Axis *GST* 1-year mortality prediction. Multi-variate Cox proportional-hazards regression analysis was performed (Table 3) on these four variables demonstrated a high concordance of 0.732; this indicates a high probability for any two randomly selected subjects, the subject with the shorter survival time has a larger risk score.

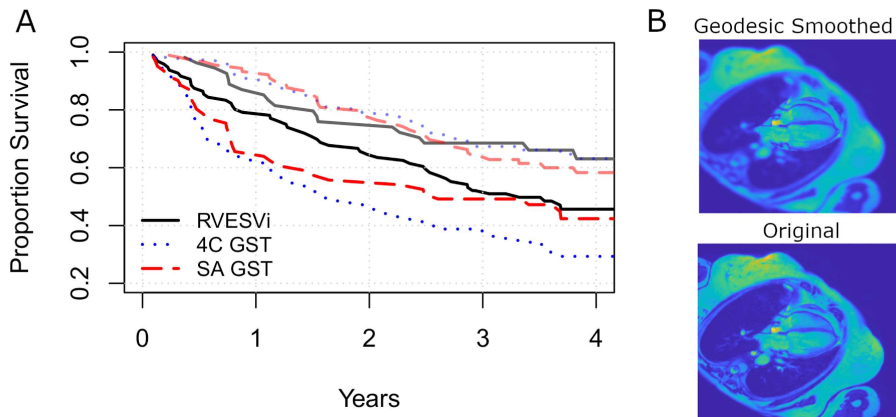


Fig. 2: A) Kaplan–Meier survival plots with standard right ventricular end-systolic volume index (RVESVi), and geodesic smoothing tensor Four Chamber (4C GST) and Short Axis (SA GST) predictions of survival through four years census. Higher curves with 50% transparency are subjects predicted-survival and lower curves at 0% transparency are subjects predicted-deceased. B) Example of geodesic smoothing (top) on a Four Chamber scan (bottom).

Table 3: Multivariate Cox proportional-hazards regression analysis. *WHO*: World Health Organization; *HR*: Hazards Ratio; *GST*: Geodesic Smoothed Tensor.

Attribute	Beta Coefficient	HR	<i>p</i>
Age	0.046 ± 0.011	1.05	< 0.01
WHO Functional Class	0.635 ± 0.301	1.89	0.04
Four Chamber GST	0.937 ± 0.246	2.55	< 0.01
Short Axis GST	0.374 ± 0.245	1.45	0.13

Limitations. The current study was limited by the relatively small cohort (150 subjects, 27 cases of 1-year mortality). Mortality is affected not only by a subject’s disease but also by lifestyle habits and treatment decisions, therefore it is possible there are levels of mortality risk (i.e. a novel virus, accident) that cannot ever be fully accounted in a prognostic assessment. We selected to extract features from two common scanning protocols (Four Chamber and Short Axis); in clinic there are additional CMRI acquisitions typically acquired which could be explored for additional or supplemental prognostic features.

4 Conclusions

This paper proposed a **Geodesically Smoothed Tensor** feature learning method (GST) which uses both the heart and its surrounding tissues for PAH prognosis. We have demonstrated that 1) tensor-based CMRI features can achieve higher

PAH mortality prediction compared to standardized measures of ventricular volume, and 2) the full GST pipeline including surrounding tissues can further improve the performance, particularly on Four Chamber scans of the heart. Further study is therefore warranted to investigate if this improvement persists in a larger cohort and for other scanning protocols.

Acknowledgements. This work was supported by the Wellcome Trust: 215799/Z/19/Z and 205188/Z/16/Z; and EPSRC: EP/R014507/1.

References

1. Bello, G.A., Dawes, T.J., Duan, J., Biffi, C., De Marvao, A., Howard, L.S., Gibbs, J.S.R., Wilkins, M.R., Cook, S.A., Rueckert, D., et al.: Deep-learning cardiac motion analysis for human survival prediction. *Nature Machine Intelligence* **1**(2), 95–104 (2019)
2. Benza, R.L., Gomberg-Maitland, M., Miller, D.P., Frost, A., Frantz, R.P., Foreman, A.J., Badesch, D.B., McGoon, M.D.: The reveal registry risk score calculator in patients newly diagnosed with pulmonary arterial hypertension. *Chest* **141**(2), 354–362 (2012)
3. Benza, R.L., Miller, D.P., Barst, R.J., Badesch, D.B., Frost, A.E., McGoon, M.D.: An evaluation of long-term survival from time of diagnosis in pulmonary arterial hypertension from the reveal registry. *Chest* **142**(2), 448–456 (2012)
4. Cox, D.R.: Regression models and life-tables. *Journal of the Royal Statistical Society: Series B (Methodological)* **34**(2), 187–202 (1972)
5. Efron, B.: Logistic regression, survival analysis, and the kaplan-meier curve. *Journal of the American statistical Association* **83**(402), 414–425 (1988)
6. Galìè, N., Humbert, M., Vachiery, J.L., Gibbs, S., Lang, I., Torbicki, A., Simonneau, G., Peacock, A., Vonk Noordegraaf, A., Beghetti, M., et al.: 2015 esc/ers guidelines for the diagnosis and treatment of pulmonary hypertension: the joint task force for the diagnosis and treatment of pulmonary hypertension of the european society of cardiology (esc) and the european respiratory society (ers): endorsed by: Association for european paediatric and congenital cardiology (aepe), international society for heart and lung transplantation (ishlt). *European Heart Journal* **37**(1), 67–119 (2016)
7. Guillevin, L.: Vasculopathy and pulmonary arterial hypertension. *Rheumatology* **48**(suppl.3), iii54–iii57 (2006)
8. Lewis, R.A., Johns, C.S., Cogliano, M., Capener, D., Tubman, E., Elliot, C.A., Charalampopoulos, A., Sabroe, I., Thompson, A.R., Billings, C.G., et al.: Identification of cardiac magnetic resonance imaging thresholds for risk stratification in pulmonary arterial hypertension. *American Journal of Respiratory and Critical Care Medicine* **201**(4), 458–468 (2020)
9. Ling, Y., Johnson, M.K., Kiely, D.G., Condliffe, R., Elliot, C.A., Gibbs, J.S.R., Howard, L.S., Pepke-Zaba, J., Sheares, K.K., Corris, P.A., et al.: Changing demographics, epidemiology, and survival of incident pulmonary arterial hypertension: results from the pulmonary hypertension registry of the united kingdom and ireland. *American Journal of Respiratory and Critical Care Medicine* **186**(8), 790–796 (2012)

10. Lu, H., Plataniotis, K.N., Venetsanopoulos, A.N.: MPCA: Multilinear principal component analysis of tensor objects. *IEEE Transactions on Neural Networks* **19**(1), 18–39 (2008)
11. Reinhold, J.C., Dewey, B.E., Carass, A., Prince, J.L.: Evaluating the impact of intensity normalization on MR image synthesis. In: *Medical Imaging 2019: Image Processing*. vol. 10949, p. 109493H. International Society for Optics and Photonics (2019)
12. Rich, J.T., Neely, J.G., Paniello, R.C., Voelker, C.C., Nussenbaum, B., Wang, E.W.: A practical guide to understanding Kaplan-Meier curves. *Otolaryngology—Head and Neck Surgery* **143**(3), 331–336 (2010)
13. Swift, A.J., Lu, H., Uthoff, J., Garg, P., Cogliano, M., Taylor, J., Metherall, P., Zhou, S., Johns, C.S., Alameddini, S., et al.: A machine learning cardiac magnetic resonance approach to extract disease features and automate pulmonary arterial hypertension diagnosis. *European Heart Journal-Cardiovascular Imaging* (2020)
14. Tustison, N.J., Avants, B.B., Cook, P.A., Zheng, Y., Egan, A., Yushkevich, P.A., Gee, J.C.: N4itk: improved N3 bias correction. *IEEE Transactions on Medical Imaging* **29**(6), 1310–1320 (2010)
15. Uthoff, J., Sieren, J.C.: Information theory optimization based feature selection in breast mammography lesion classification. In: *2018 IEEE 15th International Symposium on Biomedical Imaging (ISBI 2018)*. pp. 817–821. IEEE (2018)